Performance Enhancement of Flyback Converter's Primary Current at High Switching Frequency Utilizing Novel Input Impedance Match Technique

Muhamad Faizal Yaakub
Fakulti Teknologi dan Kejurutaraan Elektrik
Universiti Teknikal Malaysia Melaka
76100 Durian Tunggal, Melaka, Malaysia
muhamadfaizal@utem.edu.my

Mohd Amran Mohd Radzi
Advance Lightning, Power and Energy Research (ALPER) Centre
Faculty of Engineering, Universiti Putra Malaysia
43400 Serdang, Selangor, Malaysia
amranmr@upm.edu.my

Maaspaliza Azri
Fakulti Teknologi dan Kejurutaraan Elektrik
Universiti Teknikal Malaysia Melaka
76100 Durian Tunggal, Melaka, Malaysia
maaspaliza@utem.edu.my

Suhaidi Shafie
Department of Electrical and Electronic Engineering
Faculty of Engineering, Universiti Putra Malaysia
43400 Serdang, Selangor, Malaysia
suhaidi@upm.edu.my

Norhafiz Azis
Advance Lightning, Power and Energy Research (ALPER) Centre
Faculty of Engineering, Universiti Putra Malaysia
43400 Serdang, Selangor, Malaysia
norhafiz@upm.edu.my

Faridah Hanim Mohd Noh
Department of Electrical Engineering Technology
Faculty of Engineering Technology
Universiti Tun Hussein Onn Malaysia
86400 Parit Raja, Johor, Malaysia
hanim@uthm.edu.my

***Abstract*— The isolation capabilities of the flyback-based converter have garnered significant attention in different applications, particularly in photovoltaic inverter systems. However, the behavior of the anomalies, especially the parasitic element, has posed a significant difficulty in design. These irregularities ultimately interfere with the switching sequence, particularly during the current peak control operation. A novel topology is suggested to address the issue of distorted primary current during current peak control operation by leveraging the relationship between inductance and frequency in the parallel resonant circuit, as well as the input impedance of the converter. For this reason, an adaptive auxiliary path is activated during high-frequency switching. Analysis of acquiring the critical component value using the proposed input impedance match is discussed, and the alleviated result from the 100W enhanced converter topology test bench is obtained and presented.**

Keywords—converter, flyback, impedance, input current, parasitic

I. INTRODUCTION

A flyback DC-DC converter, which is schematic depicted in Fig. 1, is one of the widely utilized options for converting input DC voltage from a PV panel to a different DC voltage level when it comes to photovoltaic (PV) microinverters. The flyback transformer used in the converter is crucial in providing the converter with excellent galvanic isolation [1]–[3]. It can be sourced from commercially available options or custom-designed based on the specified switching technique, as discussed in several scholarly publications [4][5]. The transformer is designed according to a particular rating, and its specifications are carefully selected to operate within a narrow range of switching frequencies, allowing for only a limited degree of tolerance. This may pose a challenge for applications that involve varying switching frequencies. The flyback-based converter in the micro-inverter could be controlled by using one of the three modes: discontinuous conduction mode (DCM), continuous conduction mode (CCM), and boundary conduction mode (BCM). There are also several technical papers that proposed a hybrid mode combining two or more modes in one reference cycle to enhance switching performance and efficiency [6]–[9].

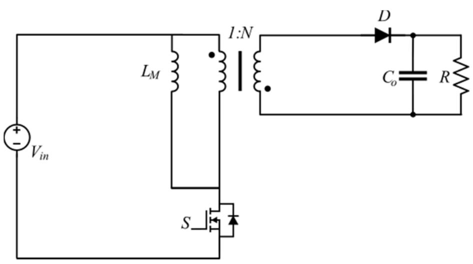

Fig. 1. Conventional flyback converter topology

Like any other system, flyback-based converters encounter their own inherent challenges, such as undesirable electrical anomalies that can potentially disrupt the circuit. Parasitic capacitance is one such anomaly. It occurs when circuit components inadvertently act as little capacitors. Its reaction with the other circuitry parasites, such as parasitic inductance, significantly increases voltage overshoot and current oscillations, which stresses the components and increases power losses from the energy conversion [10], [11]. Regrettably, this effect is significant for peak control operation, particularly with the integration of variable frequency BCM. At the corner end area of the reference signal, the BCM switching frequency is considerably high in the range of a few hundred kilo Hertz to mega Hertz. A switching signal might be triggered incorrectly due to the interfering primary current signal, resulting in ineffective power conversion. Numerous articles have proposed techniques to deal with high switching frequency at this corner end area, mainly with the switching algorithm approach [4], [12]–[14].

Another approach for reducing resonances in flyback primary current and voltage across the switching devices is to analyze and address the parasitic components. Further analysis of the transformer's behavior and response, along with that of other on-board components proposed by [1], [2], [11], [15], has the potential to enhance the overall performance. High transformation ratios magnify the resonances, which may cause changes in the anticipated primary current, and hence, impact converter behavior.

2024 IEEE Industrial Electronics and Applications Conference (IEACon) | 979-8-3503-8297-6/24/$31.00 ©2024 IEEE | DOI: 10.1109/IEACON61321.2024.10797397

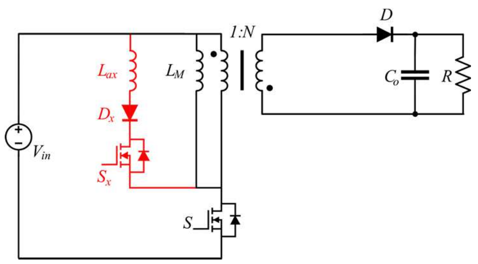

Fig. 2. Proposed enhanced flyback topology

Resonance must, therefore, be reduced to enhance the magnetizing current in flyback converters.

Various strategies have been suggested, although some are neither being used nor beneficial for flyback's current peak control operation. In [10], a parallel connected diode clamp to a series resonant inductor and switching device has been proposed to improve the sharing current on the primary side of an interleaved flyback configuration. The use of a resonant capacitor connected in parallel with the transformer's primary inductance to overcome a flyback converter's parasitic limitation is presented in [16], which was an improvement for low power level, high voltage output applications. Also, the addition of a diode clamp at a converter's input stage proposed by [17] and [18] to absorb all parasitic reactance to suit high-frequency operation, although they are not directly deployed to a flyback converter.

This paper presents a new enhanced circuit arrangement for the flyback converter and a novel technique objectively to compensate the parasitic and improve the converter's primary current at high frequency operation for peak current control, particularly involving varying switching frequency operation. This work is based on the initial investigation presented in [19] on the influence of the parasitic at the flyback transformer at high-frequency operation. Proposed enhanced circuit topology, novel input impedance match method, analysis on the circuit operation, and the related mathematical equations are discussed and presented in section II. The effectiveness of the proposed enhancement circuit and method is verified and validated through experimentation on a 100W flyback converter prototype. Results and discussion yielded from the experimental work are presented in section III.

II. Proposed Flyback Converter with Enhanced Circuit Arrangement

Given that the input current directly influences the switching mechanism, it is crucial that the current is in an appropriate shape and devoid of any distortion caused by the parasitic elements. Therefore, a novel method is proposed to attain the desired input current shape for current peak control or any protocol that necessitates a well-shaped input current throughout a wide range of switching frequencies. The fundamental principle of the proposed technique is derived from the conventional resonant circuit. The reactance of an inductor has a linear relationship with the operational frequency and exhibits an upward trend as the operational frequency is raised. However, the inductance X_L itself exhibits an inverse relationship with the operational frequency *f*.

$$X_L = 2\pi f L \tag{1}$$

$$L = \frac{X_L}{2\pi f} \tag{2}$$

The diagram depicting the enhanced circuitry is presented in Fig. 2. The conventional flyback converter is enhanced by incorporating an auxiliary path. Although the auxiliary circuit is set in with a resonance inductor, the configuration differs from what is presented in previous work [10], [20]. The proposed method is designed with the auxiliary inductance connected in parallel to the transformer's primary inductance and the converter's equivalent capacitance. Parallel connection offers greater flexibility than its series counterpart, particularly when dealing with high switching frequency adjustments. This is due to the inverse proportionality relationship between inductance and frequency, as explained in the resonance circuit fundamental. In addition to the auxiliary inductor, the proposed auxiliary path consists of a low-side power switch and a diode. The MOSFET, which functions as the low-side power switch, activates the additional pathway as needed. The parallel auxiliary inductance is activated when the transformer operates outside its designated switching frequency range. To ensure unidirectional current flow through the auxiliary path, the diode is positioned in reverse orientation relative to the anti-parallel diode of the MOSFET. Incorporating and linking extra paths in a parallel manner makes handling multiple high switching frequencies possible. The dedicated switching devices activate each path at its desired switching frequency.

The auxiliary inductance, L_{ax} is a crucial parameter in the enhanced circuitry. A new method is proposed to achieve precise and efficient estimation of component values in the auxiliary path. The process of acquiring the L_{ax} value commences by examining the input impedance, Z_{in_ref}, when the converter works at the designed operating switching frequency of the transformer specified by the manufacturer. Z_{in_ref} is defined as a reference input impedance and determined through empirical testing using an LCR meter to measure its value or through mathematical computation with data provided in the transformer datasheet and the following equation.

$$Z_{in\_ref} = \sqrt{\frac{L_{m\_opr}}{C_{eq\_opr}}} \tag{3}$$

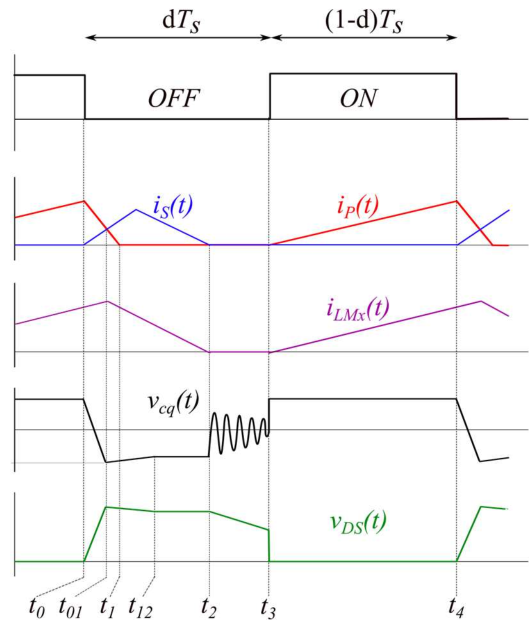

Fig. 3. Enhanced approach theoretical operation waveform under DCM

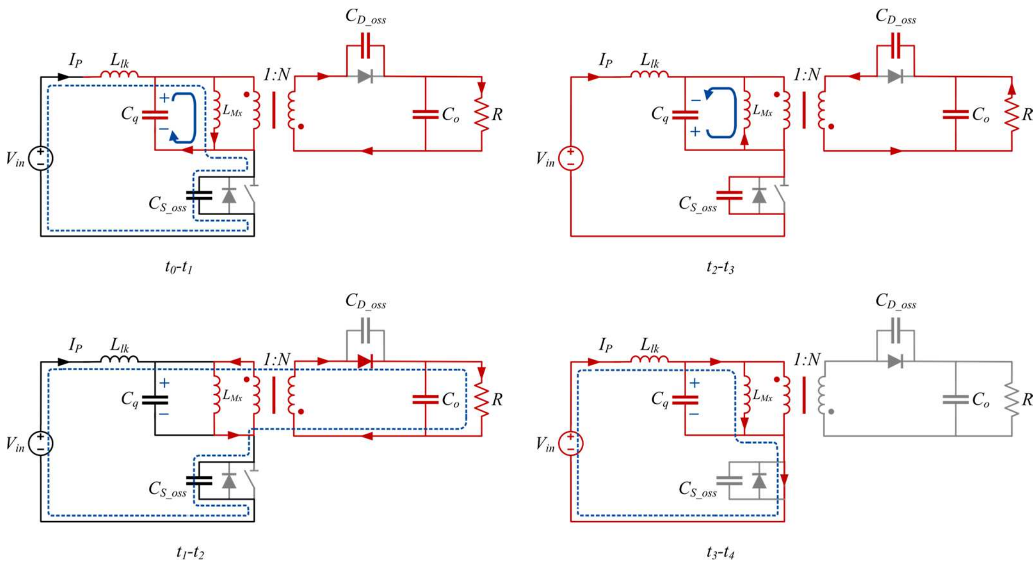

Fig. 4. Equivalent circuitry for each interval operation

where L_{m_opr} and C_{eq_opr} are the magnetizing inductance and equivalent capacitance of the transformer at its designated operation switching frequency, respectively. To determine the L_{m_opr}, it is necessary to know both the leakage inductance, L_{lk_opr}, and the primary inductance, L_{p_opr}, of the transformer. Typically, the device's datasheet provides information of these parameters. Alternatively, the values of these parameters are acquired through physical measurement [19].

$$L_{m\_opr} = \left|L_{p\_opr} - L_{lk\_opr}\right| \tag{4}$$

Meanwhile, the equivalent capacitance, C_{eq_opr}, is the total capacitance, including what is present at the secondary side of the converter, with the following relation.

$$C_{eq\_opr} = C_q + C_{S\_oss} + N^2 C_{D\_oss} \tag{5}$$

where C_q is the input capacitance, C_{S_oss} is the MOSFET output capacitance, C_{D_oss} is the diode capacitance, and N is the transformer's turn ratio. Since the parameters of the transformer are drifting relative to the switching frequency, the transformer's primary inductance, L_{p_HF}, and equivalent capacitance, C_{eq_HF}, at the new switching frequency, are required to find the L_{ax} value. Again, these parameter values are obtained through empirical measurement. The calculation of L_{ax} begins by taking the reference impedance at the operational switching frequency as an input impedance of the new switching frequency. Therefore, the relationship can be deducted as follows:

$$Z_{in\_HF} = Z_{in\_ref} = Z_{in} \tag{6}$$

From (3) and (6), the input impedance with an auxiliary path connected to the conventional circuit is formulated as follows.

$$Z_{in} = \sqrt{\frac{L_{p\_HF} || L_{ax}}{C_{eq\_HF}}} \tag{7}$$

Solving (7), the required auxiliary inductance for the enhanced flyback converter circuit can be deduced as follows.

$$L_{ax} = \frac{Z_{in}^2 C_{eq_{HF}} L_{p_{HF}}}{L_{p_{HF}} - \left(Z_{in}^2 C_{eq_{HF}}\right)} \tag{8}$$

Once the switching frequency hits the threshold value, the auxiliary circuit's low side switch is enabled, and the L_{ax} engages with the transformer. At this moment, L_m and L_{ax} produce the equivalent inductance L_{Mx}. Fig. 3 and Fig.4 show the operational waveform and the equivalent circuitry for each operation interval, respectively.

Interval 1 (t_0- t_1): The main switch, S, is in the ON position prior to switching time t_0. When the switch S is turned off at time $t = t_0$, L_{Mx} discharges the C_q. The resonance between C_q and L_{Mx} delays the passage of energy to the secondary winding until C_q reaches $-V_o/N$ and at time $t = t_1$. During this interval, the L_{lk}, simultaneously releases the energy it has been holding onto and produces the damped resonance through C_{S_oss} and internal winding resistance. The magnitude of the electrical current passing through the magnetizing-auxiliary inductance reached its maximum at t_{01}. The magnetizing-auxiliary current and the dissipated energy resulting from the presence of leakage inductance during this time period can be mathematically represented as:

$$i_{L_{Mx}}(t) = \frac{V_{in}}{Z_i}\sin(\omega_r t) + I_{LMx\_t0}\cos(\omega_r t) \tag{9}$$

$$E_{L_{lk}} = \frac{1}{2} L_{lk}\left(I_{LMx\_t0}\right)^2 \tag{10}$$

where I_{LMx_t0} is current flowing through L_{Mx} at switched off. $Z_i = \sqrt{L_{Mx}/C_q}$ and $\omega_r = 1/\sqrt{L_{Mx}C_{eq}}$.

Interval 2 (t_1 – t_2): At the instant when the equivalent voltage across the capacitor, V_{Cq}, reaches a value of $-V_o/N$ at time t_1, the diode, D, located at the secondary side of the converter is triggered into conduction. This enabled the flow of current from L_{Mx} to pass through the output side. During this particular interval, V_{cq} increases until the voltage across the main switch reaches $V_{in} + (N_1/N_2)V_o$ at t_{12}. After that, V_{cq} holds its value while the current I_{LMx} experiences a gradual decrease and eventually reaches zero at t_2. The decline in current can be mathematically represented by

$$i_{L_{Mx}}(t) = -\frac{V_o}{NL_{Mx}}(t - t_1) + I_{LMx_{t1}} \tag{11}$$

where V_o represents the converter's output voltage and I_{LMt1} indicates the current flowing via L_{Mx} at time t_1.

Interval 3 ($t_2 - t_3$): The resonance circuit is established by the capacitance and inductance, i.e., C_q, C_{S_oss}, C_{D_Oss}, L_{Mx}, *and* L_{lk} once the energy from the L_{Mx} has been fully transferred to the secondary side of the converter. At the present moment, there was a reversal in the initial voltage across the capacitor C_q, leading to a change in its polarity. Additionally, the diode on the secondary side ceased conducting when the I_{LMx} reached zero. Nevertheless, the voltage across the switch does not instantly drop to zero at this very moment. The interaction between magnetizing inductance L_{Mx} and equivalent capacitance C_q leads to a state of quasi-resonance, which aids in achieving a V_{ds} value of zero at time t_3. Consequently, the anti-parallel diode associated with the primary switch S initiates conduction, thereby facilitating the occurrence of zero voltage switching (ZVS). The magnetizing current and voltage across equivalent capacitance are deducted as:

$$i_{L_M}(t) = -\frac{V_o}{NZ_i}\sin(\omega_r t) \tag{12}$$

$$v_{C_{eq}}(t) = -\frac{V_o}{N}\cos(\omega_r t) \tag{13}$$

The termination of this interval occurs when the voltage across the equivalent capacitance V_{ceq} reaches the value of V_{in} at t_3.

Interval 4 ($t_3 - t_4$): In this interval, the switch S is activated. The electric energy accumulated at the magnetizing-auxiliary inductance, L_{Mx}, through the $V_{in} - L_{Mx} - S$ route. At once, the primary-side current rises linearly. The flowing magnetizing-auxiliary current is deducted as:

$$i_{L_{Mx}}(t) = \frac{V_i}{L_{Mx}}(t - t_3) + I_{LMx_{t3}} \tag{14}$$

where I_{Lmxt3} is the instantaneous i_{LMx} at the beginning of this interval. Current at t_4 and t_0 of the magnetizing-auxiliary inductance is eventually equal; therefore, considering (12), the equation (14) can be deducted as follows.

$$\begin{aligned} i_{L_{Mx}}(0) &= \frac{V_i}{L_{Mx}}(t_4) + I_{LMx_{t3}} \\ &= \frac{V_i}{Z_i}(\omega_r t_4) - \frac{V_o V_i}{NZ_i V_i}\sin(\omega_r t_3) \end{aligned} \tag{15}$$

The conversion ratio, Γ is defined as $\Gamma = -V_o/NV_{in}$, therefore,

$$i_{L_{Mx}}(0) = \frac{V_i}{Z_i}[(\omega_r t_4) - \Gamma\sin(\omega_r t_3)] \tag{16}$$

The end of this interval is when the primary switch S is deactivated.

III. Experimental Result

To validate the effectiveness of the new enhanced converter circuit and its method on the input current, a 100W flyback converter prototype module has been built as shown in Fig. 5 with the specifications listed in Table I. From (8) and a measured value at 160 kHz switching frequency of Z_{in_ref} = 15.2 Ω, L_{p_HF} = *-218.31 uH*, L_{lk_HF} = 1.46 *uH*, and C_{eq_HF} = *4.49 nF*, the final auxiliary inductance L_{ax} was selected as 15.6 *uH*.

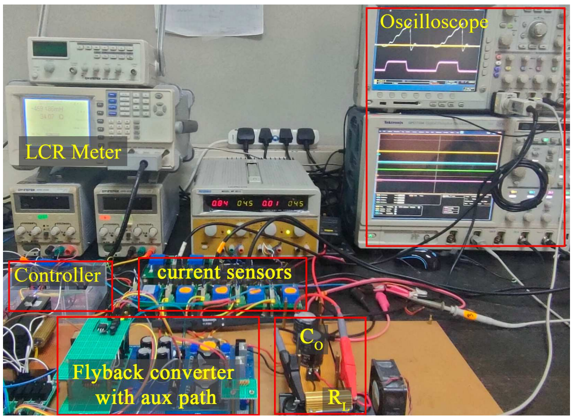

Fig. 5. Experimental setup

The master switch's switching pulse and the auxiliary's enable bit are programmed via the ePWM module of the Texas Instrument's TMS320F28379D DSP board. The experiment is conducted at 160 kHz and 200 kHz switching frequencies. The selection of testing frequencies is determined by considering the possible existence of parasitic elements and the preliminary examination of the self-resonant frequency (SRF) value.

TABLE I. Parameter of Flyback Converter

Parameter	Value	Unit
Input Voltage, V_i	30	V
Output Capacitance, C_o	940	µF
Output Resistance, R_L	1000	Ω
MOSFET Output Capacitance, C_{oss}	101.4	pF
Diode Internal Capacitance, C_D	30.93	pF

Based on the earlier investigation, the transformer under test has entered its capacitive region when operated above 150 kHz and beyond. This indicates that the SRF of the transformer is shifted to a lower value when it runs at higher frequency [19]. The experimental results of the flyback

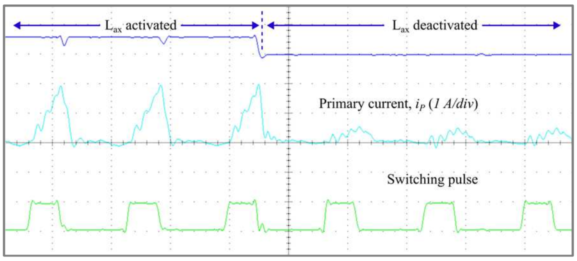

Fig. 6. 160 kHz switching frequency under DCM

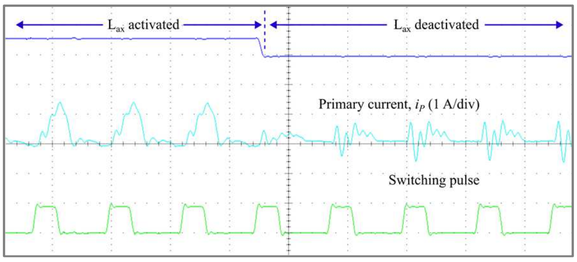

Fig. 7. 200 kHz switching frequency under DCM

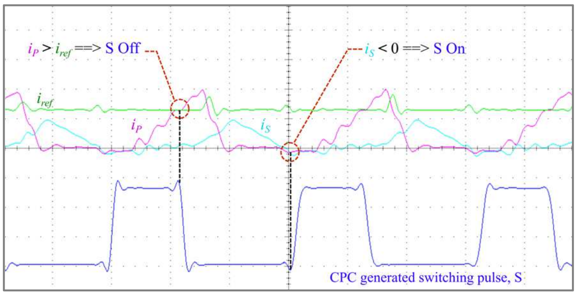

Fig. 8. Current peak control at 160 kHz switching with activated L_{ax}

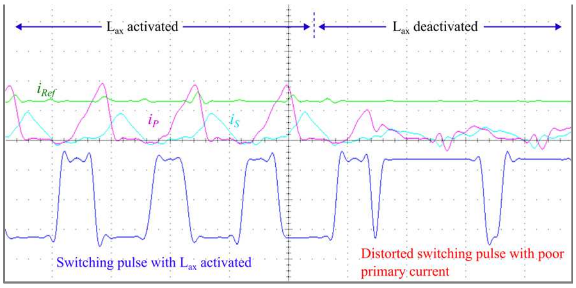

Fig. 9. Current peak control behavior with and without L_{ax}

converter with the proposed auxiliary impedance match path are presented in Fig. 6-9.

The primary current i_P response of the converter is displayed in Fig. 6 and Fig. 7, respectively, when the auxiliary path is activated and deactivated with the main switch *S* gating signal operating at 160 kHz and 200 kHz. The primary current profile during the L_{ax} engagement through the auxiliary switch is displayed in the first three pulses of Fig. 6 and Fig. 7. At this point, the peak current has an appropriate shape for peak current control operation, reaching 2 A at 160 kHz and 1.5 A at 200 kHz switching frequency. In contrast, when the converter operates at the high frequency switching operation using its conventional architecture, the primary current is obviously distorted and much reduced in amplitude.

Fig. 8 illustrates the peak current control behavior of the flyback dc-dc converter in both the conventional arrangement and the proposed input impedance match enhancement configuration under DCM. The main switch's gating signal is disrupted when the converter runs at high frequency switching with the conventional configuration, in which the L_{ax} is disengaged. From the image, it is evident that glitches occur randomly and generate an erroneous switching pulse for the converter's main switch. Once the auxiliary line is connected and L_{ax} activated, the peak current control effectively regulates and delivers an appropriate switching signal to the converter's main switch.

The current peak control operation when the auxiliary path is linked to the converter is illustrated in Fig. 9, with i_{ref} serving as the current reference for the peak current control. At this point, the gating signal for the main switch S is determined by the values of i_p and i_{ref}. The switching signal is switched to low when the input signal i_p reaches and surpasses the reference current i_{ref}. It will remain low until the zero current switching is achieved by controlling the current on the secondary side of the converter. The signal is switched to a high state during zero current switching when i_s less than zero.

IV. Conclusion

This article proposes a solution to improve the flyback converter's input current shape that disrupted the current peak control operation. It was essential to mitigate the ringing primary current of the flyback converter caused by the interaction between parasitic elements, as it affected the converter's behavior during current peak control operation. The effect of the parasitic interaction was studied in the previous work, and based on that, a new enhancement circuit for the converter to work at high frequency was introduced. The enhanced circuit was designed based on the new input impedance match technique. The analysis led to introducing the auxiliary path, consisting of L_{ax} linked in parallel with the flyback transformer's magnetizing inductance. The laboratory prototype was used to validate the theoretical conclusion. The experimental measurements of the prototype exhibit a correlation with the theoretical analysis. Moreover, an enhanced input current magnitude with an appropriate waveform, specifically for the current peak control operation, was achieved.

Acknowledgment

This work was supported under a research grant GP-IPB/2020/9688702. The authors would like to tribute special thanks to Universiti Teknikal Malaysia Melaka and Universiti Putra Malaysia for their financial and technical support.

References

[1] H. C. Mendivil, L. J. C. Ruiz, J. A. Beristain J, and J. Perez R., "Analysis of the High Gain DC-DC Converters including Parasitic Elements in Photovoltaic Systems," 2020 IEEE Int. Autumn Meet. Power, Electron. Comput. ROPEC 2020, no. Ropec, 2020, doi: 10.1109/ROPEC50909.2020.9258704.

[2] M. Li, B. Zhang, and D. Qiu, "Sneak circuit analysis for a DCM flyback DC-DC converter considering parasitic parameters," 2016 IEEE 8th Int. Power Electron. Motion Control Conf. IPEMC-ECCE Asia 2016, vol. 1, pp. 1151–1155, 2016, doi: 10.1109/IPEMC.2016.7512450.

[3] A. A. Mohammed and S. M. Nafie, "Flyback converter design for low power application," Proc. - 2015 Int. Conf. Comput. Control. Networking, Electron. Embed. Syst. Eng. ICCNEEE 2015, vol. 0, no. 1, pp. 447–450, 2016, doi: 10.1109/ICCNEEE.2015.7381410.

[4] M. Gao, M. Chen, C. Zhang, and Z. Qian, "Analysis and implementation of an improved flyback inverter for photovoltaic AC module applications," IEEE Trans. Power Electron., vol. 29, no. 7, pp. 3428–3444, 2014, doi: 10.1109/TPEL.2013.2279266.

[5] I. Variable, S. Tal, and T. Garcia, "(12) United States Patent (10) Patent No .:," vol. 2, no. 12, 2011.

[6] G. C. Christidis, A. C. Nanakos, and E. C. Tatakis, "Hybrid Discontinuous/Boundary Conduction Mode of Flyback Microinverter for AC-PV Modules," IEEE Trans. Power Electron., vol. 31, no. 6, pp. 4195–4205, 2016, doi: 10.1109/TPEL.2015.2470094.

[7] S. Kim, S. H. Lee, J. S. Lee, and M. Kim, "Dual-mode flyback inverters in gridconnected photovoltaic systems," IET Renew. Power Gener., vol. 10, no. 9, pp. 1402–1412, 2016, doi: 10.1049/iet-rpg.2015.0491.

[8] T. Lodh, N. Pragallapati, and V. Agarwal, "Novel Control Scheme for an Interleaved Flyback Converter Based Solar PV Microinverter to Achieve High Efficiency," IEEE Trans. Ind. Appl., vol. 54, no. 4, pp. 3473–3482, 2018, doi: 10.1109/TIA.2018.2818655.

[9] C. C. Chuang, C. C. Hua, C. Y. Huang, and L. K. Jhou, "Modeling a dual-mode controller design for a quasi-resonant flyback converter," Appl. Sci., vol. 9, no. 9, 2019, doi: 10.3390/app9091860.

[10] J. M. Jiménez-Martínez, E. de Jódar, and J. Villarejo, "Parasitic Capacitance Effects on Active Clamp Flyback Output Characteristics: Application to IPOP Connection," Energies, vol. 15, no. 9, 2022, doi: 10.3390/en15093201.

[11] D. Leuenberger and J. Biela, “Accurate and computationally efficient modeling of flyback transformer parasitics and their influence on converter losses,” 2015 17th Eur. Conf. Power Electron. Appl. EPE-ECCE Eur. 2015, pp. 1–10, 2015, doi: 10.1109/EPE.2015.7309194.

[12] S. J. Yaqoob et al., “Flyback Photovoltaic Micro-Inverter with a Low Cost and Simple Digital-Analog Control Scheme,” Energies, vol. 14, 2021.

[13] S. Arab Ansari, J. S. Moghani, and M. Mohammadi, “Analysis and implementation of a new zero current switching flyback inverter,” Int. J. Circuit Theory Appl., vol. 47, no. 1, pp. 103–132, 2019, doi: 10.1002/cta.2577.

[14] Z. Zhang, M. Chen, W. Chen, and Z. Qian, “Design and Analysis of the synchronization control method for BCM/DCM current-mode flyback micro-inverter,” Conf. Proc. - IEEE Appl. Power Electron. Conf. Expo. - APEC, pp. 68–75, 2013, doi: 10.1109/APEC.2013.6520187.

[15] R. Mottet, M. Almanza, A. Boegli, and Y. Perriard, “Critical Parasitic Elements of Coupled Inductors for Ultra-High Voltage Flyback Converters Used to Drive Capacitive Actuators,” 2019 22nd Int. Conf. Electr. Mach. Syst. ICEMS 2019, pp. 1–5, 2019, doi: 10.1109/ICEMS.2019.8921772.

[16] S. S. Hong, S. K. Ji, Y. J. Jung, and C. W. Roh, “Analysis and design of a high voltage flyback converter with resonant elements,” J. Power Electron., vol. 10, no. 2, pp. 107–114, 2010, doi: 10.6113/JPE.2010.10.2.107.

[17] M. Masihuzzaman and N. Lakshminarasamma, “An improved ZVS-PWM, active clamp/reset forward converter: Analysis, design and dynamic model,” 2010 IEEE 12th Work. Control Model. Power Electron. COMPEL 2010, vol. 1, pp. 1–8, 2010, doi: 10.1109/COMPEL.2010.5562442.

[18] C. M. C. Duarte and I. Barbi, “An improved family of ZVS-PWM active-clamping DC-to-DC converters,” PESC Rec. - IEEE Annu. Power Electron. Spec. Conf., vol. 1, no. 1, pp. 669–675, 1998, doi: 10.1109/PESC.1998.701970.

[19] M. F. Yaakub, M. Amran, M. Radzi, F. Hanim, and M. Noh, “Simulation of DC-DC Converter Considering Parasitic Element in Flyback Transformer and its Effect on the Converter ’ s Input Current,” 2023 IEEE 11th Conf. Syst. Process Control, vol. 1, no. December, pp. 182–187, 2023, doi: 10.1109/ICSPC59664.2023.10420409.

[20] S. A. Ansari and J. S. Moghani, “Soft switching flyback inverter for photovoltaic AC module applications,” IET Renew. Power Gener., vol. 13, no. 13, pp. 2347–2355, 2019, doi: 10.1049/iet-rpg.2019.0365.